Eur. J. Mineral.
2006, **18**, 691–704

Order and anti-order in olivine II: Thermodynamic analysis and crystal-chemical modelling

HERBERT KROLL[1], ARMIN KIRFEL[2] and ROLF HEINEMANN[1]

[1]Institut für Mineralogie, Westfälische Wilhelms-Universität, Corrensstr. 24, 48149 Münster, Germany
*Corresponding author, e-mail: kroll@nwz.uni-muenster.de
[2]Mineralogisch-Petrologisches Institut, Poppelsdorfer Schloss, 53115 Bonn, Germany

Abstract: The equilibrium order/anti-order behaviour in olivine $Fe_{0.48}Mg_{0.52}[SiO_4]$ is analysed in terms of the Thompson (1969, 1970) model for the Gibbs energy due to ordering, G^{ord},

$$G^{ord} = -\frac{1}{2}\Delta G^0_{exch}\, Q - TS^{ord}_{conf}.$$

$\Delta G^0_{exch} = \Delta H^0_{exch} - T\Delta S^0_{exch}$ relates to the exchange reaction $Fe^{M2} + Mg^{M1} \leftrightarrow Fe^{M1} + Mg^{M2}$. Since for the investigated olivine both ΔH^0_{exch} and ΔS^0_{exch} are positive (ΔH^0_{exch} = 1.2 kJ/mol, ΔS^0_{exch} = 3.7 J/mol K), an ordered Fe^{2+},Mg configuration is favoured by the enthalpic part of ΔG^0_{exch} whereas the vibrational entropic part favours anti-ordering. As a result, at low temperatures, where $\Delta H^0_{exch} > T\Delta S^0_{exch}$, Fe^{2+} prefers M2. Since, however, the energy $T\Delta S^0_{exch}$ steadily increases with increasing temperature it promotes Fe^{2+} into M1 and full disorder is attained at a crossover temperature T_{co} where $\Delta H^0_{exch} = T_{co}\, \Delta S^0_{exch}$. Above T_{co}, $T\Delta S^0_{exch}$ becomes progressively larger than ΔH^0_{exch} and stimulates further fractionating of Fe^{2+} into M1 corresponding to increasing anti-order. The unusual phenomenon of anti-order increasing at increasing temperatures is due to ΔH^0_{exch} being relatively small in FeMg olivine compared to the temperature proportional energy $T\Delta S^0_{exch}$. In other AB olivines (A, B = Mn, Fe, Co, Ni, Mg) the exchange enthalpies are much larger, between 9 and 20 kJ/mol, so that they dominate ΔG^0_{exch} to a degree that precludes a crossover from ordered to anti-ordered states up to the melting point.

The exchange enthalpies reported for MnMg, FeMg, CoMg, NiMg and MnFe olivines can be rationalized in terms of cation radius (r) and electronegativity (χ) ratios of the A and B cations. In a novel approach, both radii and electronegativities have been derived from topological analyses of the procrystal electron density distributions of pure $M_2[SiO_4]$ olivines (M = Mn, Fe, Co, Ni, Mg) yielding a very satisfactory description by

$$\Delta H^0_{exch} = 252.6(\pm 6.1)\,[r(A)/r(B) - 1] - 75.8(\pm 1.9)\,[\chi(A)/\chi(B) - 1].$$

Accordingly, the small value of ΔH^0_{exch} found for FeMg olivine is a consequence of opposite radius and electronegativity contributions which almost cancel. In MnFe olivine, although both contributions are small, they cooperate resulting in a moderate value of ΔH^0_{exch}. In MnMg olivine, it is the radius ratio that dominates, contrary to CoMg and NiMg olivine where the electronegativity ratios control ΔH^0_{exch}. Consequently, Mn prefers M2, and Co and Ni segregate into M1.

ΔS^0_{exch} can be split into vibrational, $\Delta S^{0,vib}_{exch}$, and electronic exchange entropies, $\Delta S^{0,el}_{exch}$. Describing the first in terms of a new octahedral distortion parameter, D_f, and estimating the second from the Boltzmann distribution of the 3d-electrons, ΔS^0_{exch} can be satisfactorily modelled by

$$\Delta S^0_{exch} = 35.76(\pm 0.34)\,\{[D_f(A)^{M1} + D_f(B)^{M2}]/[D_f(B)^{M1} + D_f(A)^{M2}] - 1\} + \Delta S^{0,el}_{exch}$$

The resulting $\ln K_D = -(\Delta H^0_{exch} - T\Delta S^0_{exch})/RT$ allows, for the first time and to the best of our knowledge, an exclusively electron density based description of the experimentally observed temperature variations of the site occupancies in AB olivines. This modelling of $\ln K_D$ allows also for predicting the temperature variation of equilibrium cation distributions in AB olivines not investigated so far.

Key-words: olivine, order, anti-order, thermodynamic analysis, exchange enthalpy, nonconfigurational entropy, electronic entropy, topological analysis, ionic radius, electronegativity.

Introduction

The distribution of two-valent cations over the two non-equivalent M1 and M2 octahedral sites of the olivine structure has been the subject of numerous investigations. So far detailed knowledge about the variation of the cation distribution with temperature is only available for five compounds: MnMg, FeMg, CoMg, NiMg and MnFe olivine

0935-1221/06/0018-0691 $ 6.30
DOI: 10.1127/0935-1221/2006/0018-0691

(Redfern *et al.*, 1997, 2000; Henderson *et al.*, 2001; Morozov *et al.*, 2001a,b, 2002, 2005; Sutanto, 2004; Sutanto *et al.*, 2004; Heinemann *et al.*, 2003a,b; 2006). Except for FeMg olivine, all these compounds behave in agreement with expectation exhibiting progressive disorder with increasing temperature, whereas FeMg olivine does the opposite. In the following, we commence with discussing the order/anti-order behaviour of Fe,Mg olivine within the framework of the solid solution model of Thompson (1969, 1970). Then, the extraordinary behaviour of this compound will be compared with that of the other four AB olivines, and the crystal-chemical factors affecting site preferences will be discussed. Modifying the approach of Tsukimura & Sasaki (2000) we show that the enthalpy of the exchange reaction

$$A^{M2} + B^{M1} \underset{\text{order}}{\overset{\text{anti-order}}{\rightleftharpoons}} A^{M1} + B^{M2} \tag{1}$$

can be modelled and rationalized in terms of the ionic radii and electronegativity ratios of the two-valent A and B cations. These ratios can be derived from well-known tables (e.g. Shannon & Prewitt, 1970; Shannon, 1976; Allred & Rochow, 1958). The recent progress in charge density analysis offers, however, the alternative of deriving cation radii, r(Å), and electronegativity values, χ, on the basis of the actual charge density distributions. Since these are already reasonably well approximated (Gibbs *et al.*, 1997) by the procrystal density (i.e. the independent atom model) we have chosen this latter approach, both to put it to test and to make use of its potential to extract bond specific properties, r and χ.

In addition to the exchange enthalpy, we are also able to describe the exchange entropy of reaction (1) in terms of structure properties, viz. octahedral face distortions. This modelling of both exchange enthalpies and entropies allows for predicting site occupancies and their variation with temperature for AB olivines not yet thermally investigated.

Order and anti-order in Fe,Mg olivine

The Thompson model

In his treatment on chemical reactions in crystals, Thompson (1969, 1970) suggested that in the Gibbs energy expression for a solid solution, which undergoes cation ordering, the configurational entropy S_{conf} be separated from the non-configurational entropy $S_{non\text{-}conf}$,

$$G = H - (TS_{non\text{-}conf} + TS_{conf}). \tag{2}$$

While the molar configurational entropy in olivines is conventionally written as,

$$S_{conf} = -R(X_A^{M2} \ln X_A^{M2} + X_B^{M2} \ln X_B^{M2} + X_A^{M1} \ln X_A^{M1} + X_B^{M1} \ln X_B^{M1}), \tag{3}$$

$(H - TS_{non\text{-}conf})$ requires modelling by a suitable function, e.g. a second-order Taylor expansion in terms of both a composition dependent variable

$$X = X_A^{M1} + X_A^{M2} - 1 = 2X_A - 1 \tag{4}$$

and a long-range order parameter

$$Q = X_A^{M2} - X_A^{M1}. \tag{5}$$

Q may vary between -1 and +1. Q = -1 denotes an anti-ordered $B^{M2}A^{M1}[SiO_4]$ configuration, Q = +1 an ordered $A^{M2}B^{M1}[SiO_4]$ configuration, and Q = 0 denotes complete disorder. The coefficients of the Taylor expansion can be evaluated in terms of familiar thermodynamic quantities (Sack & Ghiorso, 1989; Kroll *et al.*, 1994). The resulting expression for G may be split into two parts, one that describes the free energy of a fully disordered olivine and another one, we are actually interested in, that models the free energy gain due to ordering,

$$\begin{aligned} G^{ord} &= G_Q - G_{Q=0} \\ &= -\frac{1}{2}[\Delta G^0_{exch} - (L^G_{M1} - L^G_{M2})X]Q \\ &\quad + \frac{1}{4}[\Delta G^0_{rec} - (L^G_{M1} + L^G_{M2})]\,Q^2 - TS^{ord}_{conf} \end{aligned} \tag{6}$$

The first term, linear in Q, describes a temperature and composition dependent internal field, which is dominated by the exchange Gibbs energy,

$$\Delta G^0_{exch} = G^0_{Q=-1} - G^0_{Q=1}. \tag{7}$$

$(L^G_{M1} - L^G_{M2})X$ accounts for the dependence of the field on the A,B concentrations where L^G_{M1} and L^G_{M2} are intrasite interaction parameters. The second term of equation (6), quadratic in Q, models an effective site interaction and accounts for all physical effects that lead to the coupling between occupancies at the M1 and M2 sites (e.g. nearest-neighbour interactions; Salje, 1992). This coupling is modelled by intra- and intersite interactions, the latter being expressed by the reciprocal reaction Gibbs energy,

$$\Delta G^0_{rec} = (G^0_{Q=-1} + G^0_{Q=1}) - (G^0_{Fo} + G^0_{Fa}) \tag{8}$$

where G^0_{Fo} and G^0_{Fa} are the Gibbs energies of forsterite and fayalite, respectively. At internal equilibrium, $\partial G_{ord} / \partial Q = 0$, one obtains

$$\begin{aligned} -RT \ln K_D &= \Delta G^0_{exch} - (L^G_{M1} - L^G_{M2})X \\ &\quad - [\Delta G^0_{rec} - (L^G_{M1} + L^G_{M2})]Q \end{aligned} \tag{9}$$

with

$$K_D = X_A^{M1} X_B^{M2} / X_A^{M2} X_B^{M1}. \tag{10}$$

The experimental evaluation of $\ln K_D$ *vs.* 1/T yields the parameters of equation (6). Fortunately, simplifications are possible. When the $\ln K_D$ values derived for the five AB olivines mentioned above are plotted *versus* 1/T (Fig. 1) it is evident that $\ln K_D$ relates linearly to 1/T. Therefore, the Q term in equation (9) which is capable of modelling nonlinearity has been neglected. The X term may also be neglected because X (eqn 4) is zero or very close to zero for all five compounds so that $RT \ln K_D \approx RT \ln K_{exch}$. Thus, equations (6) and (9) can be shortened to give

$$G^{ord} = -\frac{1}{2}[\Delta H^0_{exch} - T\,\Delta S^0_{exch}]Q - T\,S^{ord}_{conf} \tag{11}$$

Table 1. Experimental enthalpies and entropies for the exchange reaction $A^{M2} + B^{M1} \leftrightarrow B^{M2} + A^{M1}$.

exchange reaction order Q = 1	exchange reaction anti-order Q = -1	ΔH^0_{exch} [kJ/mol]	ΔS^0_{exch} [J/mol K]	
$Mn^{M2} + Mg^{M1}$	$\leftrightarrow Mg^{M2} + Mn^{M1}$	15.64 (± 0.98)	2.12 (± 1.01)	(1)
$Fe^{M2} + Mg^{M1}$	$\leftrightarrow Mg^{M2} + Fe^{M1}$	1.16 (± 0.05)*	3.68 (± 0.06)	(2)
$Co^{M2} + Mg^{M1}$	$\leftrightarrow$ **$Mg^{M2} + Co^{M1}$**	–12.51 (± 1.03)	1.85 (± 0.97)	(3)
$Ni^{M2} + Mg^{M1}$	$\leftrightarrow$ **$Mg^{M2} + Ni^{M1}$**	–20.48 (± 1.55)	–0.52 (± 1.27)	(4)
$Mn^{M2} + Fe^{M1}$	$\leftrightarrow Fe^{M2} + Mn^{M1}$	10.14 (± 0.29)	–0.56 (± 0.29)	(5)

A configuration is termed ordered when the larger cation resides in the larger M2 site, the smaller one in the smaller M1 site. Configurations in bold-face apply to low temperatures. For cation radii see Tables 2 and 4.

ΔH^0_{exch} and ΔS^0_{exch} were obtained from eqn (12) using $\ln K_D$ values of Redfern *et al.* (1997): (1) and (5), Heinemann *et al.* (2006): (2), Sutanto (2004): (3), Henderson *et al.* (2001): (4).

* Note that according to our definition of Q being opposite to that of Redfern *et al.* (2000), their $\Delta H^0_{exch} = -11{,}1$ kJ/mol.

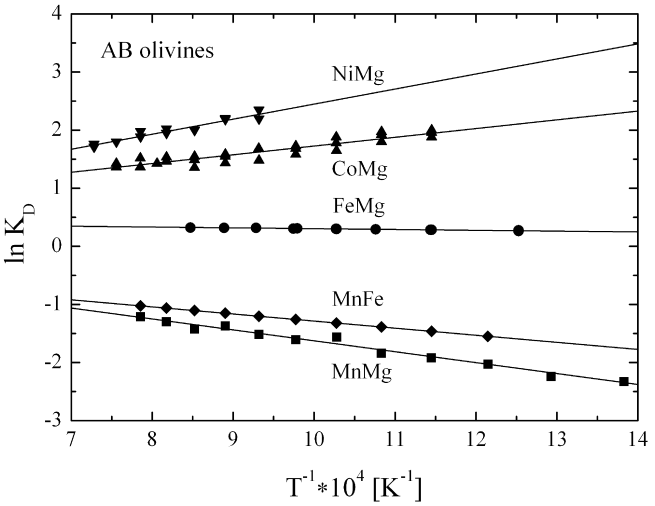

Fig. 1. Comparison of experimentally observed $\ln K_D$ *vs* 1/T relations in AB olivines: MnMg and MnFe olivine (Redfern *et al.*, 1997), FeMg olivine (Heinemann *et al*., 2006), CoMg olivine (Sutanto *et al.*, 2004), NiMg olivine (Henderson *et al.*, 2001).

and

$$-RT \ln K_D = \Delta G^0_{exch} = \Delta H^0_{exch} - T\Delta S^0_{exch} . \quad (12)$$

The exchange or site preference enthalpy, ΔH^0_{exch}, is the enthalpy difference between the anti-ordered and ordered states, $\Delta H^0_{exch} = H^0_{Q=-1} - H^0_{Q=1}$. Correspondingly, the exchange or site preference entropy, ΔS^0_{exch}, is the nonconfigurational entropy difference between these states, $\Delta S^0_{exch} = S^0_{Q=-1} - S^0_{Q=1}$. Values of ΔH^0_{exch} and ΔS^0_{exch} derived from the five $\ln K_D$ relations in Fig. 1 are listed in Table 1. The exchange reactions (left column) transform ordered states into anti-ordered ones. Ordered states are defined by the larger cation residing in the larger M2 site while the smaller cation resides in the smaller M1 site, and vice versa for anti-ordered states. The configurations in bold-face apply to low temperatures. The signs of ΔH^0_{exch} and ΔS^0_{exch} follow from the chosen direction of the site exchange (left to right).

Variation with temperature of energies contributing to G^{ord}

In FeMg olivine, $H^0_{Q=-1}$ is larger than $H^0_{Q=1}$ so that ΔH^0_{exch}, the enthalpic part of the internal field, stabilizes the ordered state at all temperatures. The entropic part, $T\Delta S^0_{exch}$, is also a positive quantity. ΔS^0_{exch} mainly encompasses vibrational exchange entropy, as argued below. Thus, $\Delta S^0_{exch} > 0$ means that the vibrational entropy of anti-ordered Fe^{2+},Mg configurations is larger than that of ordered configurations, and therefore ΔS^0_{exch} favours the anti-ordered state at all temperatures. In the low temperature region, ΔH^0_{exch} dominates ΔG^0_{exch} predicting FeMg olivine to be ordered. With rising temperature, microscopic anti-ordered Fe^{2+},Mg configurations are progressively generated due to the influence of the configurational entropy. The vibrational exchange entropy reinforces this tendency so that eventually full disorder is reached when $\Delta G^0_{exch} = \Delta H^0_{exch} - T_{co}\ \Delta S^0_{exch} = 0$, where T_{co} denotes a crossover temperature,

$$T_{co} = \Delta H^0_{exch} / \Delta S^0_{exch} . \quad (13)$$

Below T_{co}, both the configurational and exchange entropies favour anti-ordered configurations. Above T_{co}, however, they act in an antagonistic way; while the configurational entropy tries to conserve the disordered state, ΔS^0_{exch} continues to promote anti-order. The corresponding energetic relations are depicted in Fig. 2. To this purpose, equation (11) is rewritten as

$$G^{ord} = H^{ord} - T\Delta S^{ord} \quad (14a)$$

with

$$H^{ord} = H_Q - H_{Q=0} = -1/2\ \Delta H^0_{exch}\, Q \quad (14b)$$

$$S^{ord} = S_Q - S_{Q=0} = -1/2\ \Delta S^0_{exch}\, Q + S^{ord}_{conf}. \quad (14c)$$

Then, the energetic relations of the exchange reaction at the temperature of interest can be described as follows. Let us start from a state of full disorder. Then, at $T < T_{co}$ we are

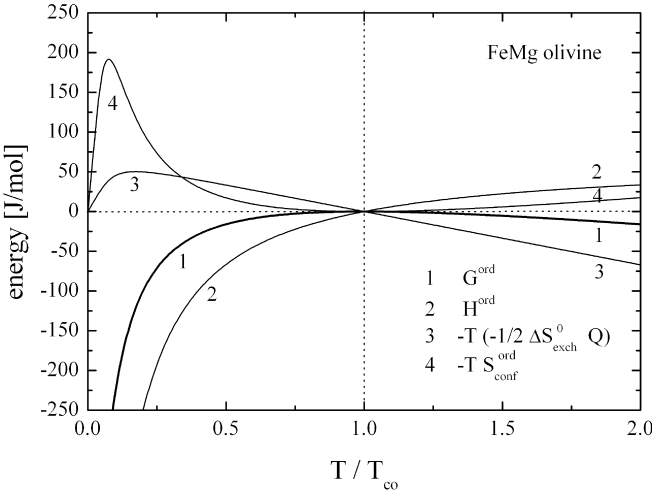

Fig. 2. FeMg olivine: Variation with temperature ratio T/T_{co} of the enthalpic, vibrational entropic and configurational entropic contributions to the Gibbs energy due to ordering, G^{ord}.

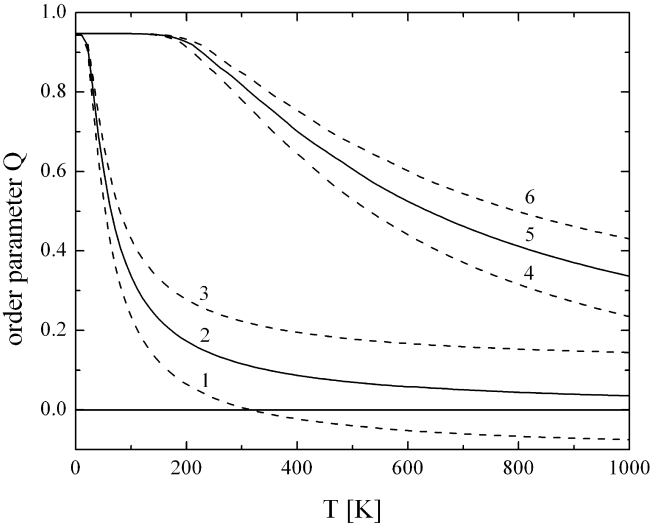

Fig. 3. Simulated variation with temperature of the order parameter Q calculated from six combinations of ΔH^0_{exch} and ΔS^0_{exch}. Curves 1, 2, 3: ΔH^0_{exch}= 1.16 kJ/mol, ΔS^0_{exch}= +3.68, 0.00, -3.68 J/molK, respectively. Curves 4, 5, 6: ΔH^0_{exch}= 11.6 kJ/mol, ΔS^0_{exch}= +3.68, 0.00, -3.68 J/molK, respectively. Curve 1 represents the observed variation of Q for FeMg olivine.

dealing with an ordering reaction leading from full disorder to partial order. The reaction is exothermic ($H^{ord} < 0$) because ordered Fe^{2+},Mg configurations have smaller energies than anti-ordered ones. It is thus an enthalpy driven reaction. The number of ordered configurations increases against the opposed influences of the configurational and exchange vibrational entropies which both decrease in the process. Thus, $-TS^{ord}_{conf}$ and $-T(-1/2\ \Delta S^0_{exch}\ Q)$ are positive in Fig. 2. In contrast, at a given temperature $T > T_{co}$ the reaction is endothermic ($H^{ord} > 0$) and leads to progressive anti-order. It is driven by the vibrational exchange entropy enforcing anti-order against the influences of the exchange enthalpy, which favours order, and against the configurational entropy, which favours disorder. Thus, H^{ord} and $-TS^{ord}_{conf}$ are positive, while $-T(-1/2\ \Delta S^0_{exch}\ Q)$ is negative. The configurational entropy decreases in both the exothermic and endothermic regimes. In the exothermic regime, it decreases in response to the exchange *enthalpy* promoting order, whereas in the endothermic regime it decreases in response to the exchange *entropy* promoting anti-order.

In general, it is the vibrational entropic difference between anti-ordered and ordered A,B configurations that characterizes the evolution of the site occupancies with temperature. As illustrated in Fig. 3 (curves 1 and 4), a crystal can reach anti-order below the melting point provided ΔH^0_{exch} and ΔS^0_{exch} are both positive and of suitable magnitudes. Conversely, for ΔH^0_{exch} and ΔS^0_{exch} both negative, anti-order may eventually turn into order. For $\Delta H^0_{exch} > 0$ and $\Delta S^0_{exch} = 0$, such a crossover cannot occur. The material simply approaches disorder (curves 2 and 5). For $\Delta S^0_{exch} < 0$, the approach to disorder is retarded (curves 3 and 6), and similarly for $\Delta H^0_{exch} < 0$ and $\Delta S^0_{exch} > 0$, disorder is approached from the state of anti-order at a lower rate than in the case of $\Delta S^0_{exch} = 0$. The general notion sometimes found in the literature that non-convergent disordering will lead to full disorder at high temperatures is not generally correct. It applies only to the case $\Delta S^0_{exch} = 0$ corresponding to the assumption that the internal field is independent of temperature.

In summary, although increasing order or anti-order at increasing temperatures is a phenomenon rarely observed it is not forbidden by thermodynamics. Whether or not such a regime exists below the melting point depends only on the ratio ΔH^0_{exch} / ΔS^0_{exch} being positive and sufficiently small. Both conditions are fulfilled for FeMg olivine. We know of only one other mineral, namely magnetite, which orders at elevated temperatures. At low temperatures, magnetite is an inverse spinel, $Fe^{3+}_t\ (Fe^{2+}\ Fe^{3+})_o\ O_4$ (t and o designate tetrahedral and octahedral sites, respectively), with an anti-ordered configuration. The change towards order follows from $\ln K_D = -2.14 + 2825/T$, i.e. $\Delta H^0_{exch} = -23.5$ kJ/mol and $\Delta S^0_{exch} = -17.8$ J/molK (Wißmann *et al.*, 1998). Although ΔH^0_{exch} is large, disorder is only attained at $T_{co} \approx 1050$ °C because ΔS^0_{exch} is large, too. Above T_{co} and up to the melting point at ≈ 1600 °C order increases.

Order/anti-order behaviour is restricted to structures that show non-convergent disordering. Those with convergent disordering cannot show this phenomenon because they do not posses an internal field. Their ordered and anti-ordered states are energetically equivalent, i.e. there are no enthalpy and nonconfigurational entropy differences between these states, and the response to reaching disorder is a structural change, i.e. a phase transition.

Order and anti-order in isotypic transition-metal, Mg olivines

Using the $\ln K_D$ parameters of Table 1 the temperature variations of the site occupancies of the five AB olivines under consideration have been calculated and plotted in Fig. 4, tacitly assuming that $\ln K_D$ *vs.* 1/T extrapolates linearly. The plot illustrates the strongly different ordering in FeMg oliv-

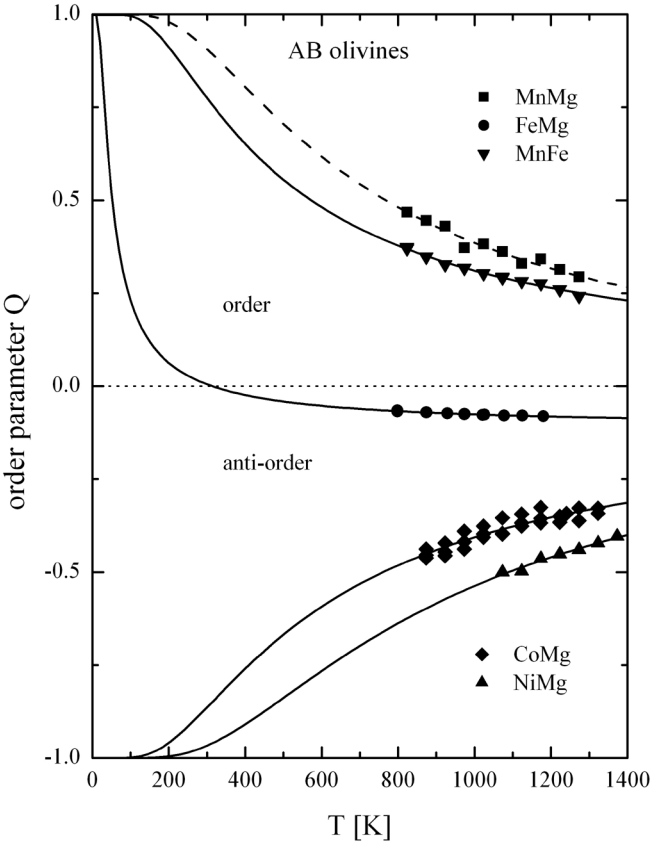

Fig. 4. Temperature variation of the order parameter $Q = X_A^{M2} - X_A^{M1}$ where A = Mn, Fe, Co, Ni, and X_A^{M1} and X_A^{M2} are site occupancies calculated from extrapolated $\ln K_D$ relations (Table 1). The data points for CoMg olivine represent three different measurements (Sutanto, 2004).

ine as compared to the other four AB olivines. FeMg olivine is close to disorder at all geologically relevant temperatures. If kinetically feasible, Fe^{2+} would fractionate into M2 only at low temperatures. In fact, only in Mg-rich olivines, in which T_{co} is higher than in FeMg olivine, Fe^{2+} has been observed to be enriched in M2 (Aikawa *et al*., 1985; Freiheit *et al*., 2000). As for FeMg olivine, the positive ΔH^0_{exch} in MnMg olivine favours ordering, while the likewise positive ΔS^0_{exch} favours anti-ordering. Unlike FeMg olivine, however, the enthalpic part of the internal field by far dominates the entropic part as is apparent from the large ratio ΔH^0_{exch} $/\Delta S^0_{exch}$ (Table 1). As a consequence, no crossover to anti-ordering can occur before melting. Nevertheless, with ΔH^0_{exch} and ΔS^0_{exch} being positive, the temperature variation of G^{ord} and its components resembles that of FeMg olivine when plotted against the normalized temperature T/T_{co} (Fig. 5). Turning back to Fig. 4, in NiMg olivine the negative exchange enthalpy promoting anti-order is opposed by a negative exchange entropy promoting order. However, similar to MnMg olivine the large ΔH^0_{exch} $/\Delta S^0_{exch}$ ratio prevents a crossover to ordering before melting. In MnFe and CoMg olivine, the signs of ΔH^0_{exch} and ΔS^0_{exch} are opposite, favouring order in MnFe and anti-order in CoMg olivine, thus preventing a crossover in both cases.

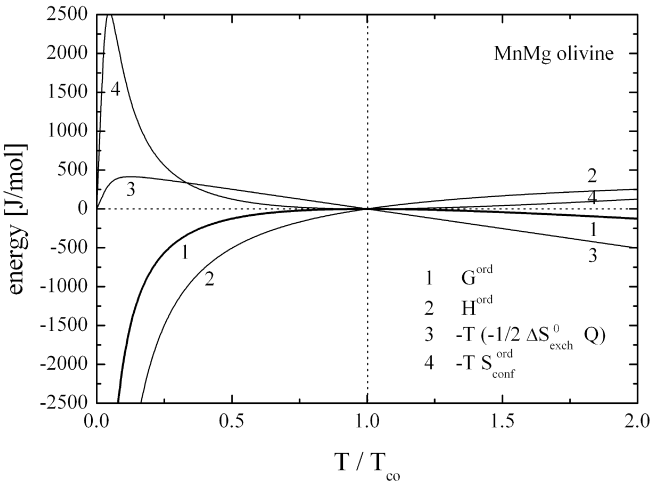

Fig. 5. MnMg olivine: Variation with temperature ratio T/T_{co} of the enthalpic, vibrational entropic and configurational entropic contributions to the Gibbs energy due to ordering, G^{ord} (compare with Fig. 2).

Modelling the cation distribution and its dependence on temperature and composition

Factors influencing site preferences

In the following, we attempt to model the magnitudes and signs of ΔH^0_{exch} and ΔS^0_{exch} in terms of structural parameters in order to further our understanding of the variation of site occupancies beyond the formal thermodynamic description.

Differing chemical properties and geometrical environments of the two-valent cations control their distribution over the M1 and M2 sites. In the literature, three factors are discussed that are considered to affect the site preferences in olivines (e.g., Burns, 1970, 1983; Walsh *et al.*, 1974, 1976; Rajamani *et al.*, 1975; Burns & Sung, 1978; Bish, 1981; Brown, 1980; Ghose, 1982; Tsukimura & Sasaki, 2000). These are

(1) The smaller of the two cation species tends to fractionate into the smaller M1 coordination octahedron (size effect).

(2) The more electronegative element segregates into the "less ionic" M1 site. (a) Bond strength calculations show that, on average, the oxygen atoms coordinating M1 are slightly overbonded compared to those coordinating M2. Hence, M1 should be favoured by the more electronegative species. (b) Charge density studies of forsterite by Tamada & Tanaka (1988) and of forsterite and fayalite by Kirfel and co-workers (Kirfel & Lippmann, 2001, 2002; Kirfel *et al*., 2003; Gibbs *et al*, 2005; Kirfel *et al*., 2005) have revealed that the Mg and Fe ions occupying M1 are less positively charged than they are on M2. Calculations of the procrystal electron density distributions (see below) show that this holds for all the studied olivines. Thus, similar to (a), the more electronegative ion will occupy the M1 site. (c) Likewise, Ghose (1982) argued that as Fe^{2+} exhibits a smaller isomer shift at M1 than at M2 (determined by Mößbauer spectroscopy; Finger & Virgo, 1971; Shinno *et al.*, 1974), the M1-O bonds possess a higher degree of covalency.

Table 2. M-O bond lengths [d(M-O)], distances M-bcp [r(M)] and bcp-O [r(O)], all in Å, and bond critical point (bcp) electron density values $\rho(\mathbf{r}_c)$ [e/Å^3] calculated for the procrystals of $M_2[SiO_4]$, M = Mn, Fe, Co, Ni, Mg. See text for the calculation of the electronegativity values χ.

bond		d(M-O)	r(M)	r(O)	$\rho(\mathbf{r}_c)$	χ
Mg1	-O1	2.0836	0.925	1.159	0.253	1.083
	-O2	2.0676	0.917	1.153	0.269	1.099
	-O3	2.1314	0.941	1.195	0.240	1.062
<Mg1-O>		2.0942	0.928	1.169	0.254	1.081
Mg2	-O1	2.1767	0.960	1.217	0.211	1.027
	-O2	2.0454	0.911	1.134	0.264	1.099
	-O3	2.0650	0.919	1.146	0.252	1.085
	-O3'	2.2101	0.970	1.245	0.207	1.017
<Mg2-O>		2.1287	0.942	1.189	0.232	1.055
<Mg-O>		2.1115	0.935	1.179	0.243	1.068
Mn1	-O1	2.2003	1.109	1.092	0.333	1.560
	-O2	2.1671	1.092	1.076	0.366	1.599
	-O3	2.2498	1.130	1.122	0.311	1.526
<Mn1-O>		2.2057	1.110	1.097	0.337	1.562
Mn2	-O1	2.2782	1.145	1.134	0.283	1.489
	-O2	2.1368	1.080	1.057	0.373	1.613
	-O3	2.1547	1.088	1.067	0.357	1.593
	-O3'	2.3194	1.163	1.159	0.269	1.465
<Mn2-O>		2.2272	1.121	1.107	0.318	1.536
<Mn-O>		2.2165	1.116	1.102	0.327	1.549
Fe1	-O1	2.1208	1.069	1.051	0.396	1.688
	-O2	2.1246	1.070	1.056	0.403	1.693
	-O3	2.2367	1.122	1.117	0.323	1.589
<Fe1-O>		2.1607	1.087	1.075	0.374	1.657
Fe2	-O1	2.2331	1.121	1.112	0.313	1.579
	-O2	2.1089	1.064	1.045	0.398	1.693
	-O3	2.0625	1.043	1.019	0.441	1.743
	-O3'	2.2931	1.149	1.146	0.286	1.536
<Fe2-O>		2.1755	1.095	1.081	0.361	1.638
<Fe-O>		2.1681	1.091	1.078	0.367	1.648
Co1	-O1	2.0937	1.048	1.046	0.406	1.747
	-O2	2.0909	1.045	1.047	0.418	1.758
	-O3	2.1689	1.081	1.090	0.357	1.680
<Co1-O>		2.1178	1.058	1.061	0.394	1.728
Co2	-O1	2.1787	1.086	1.092	0.338	1.658
	-O2	2.0725	1.038	1.034	0.416	1.761
	-O3	2.0672	1.036	1.031	0.420	1.766
	-O3'	2.2228	1.106	1.119	0.318	1.626
<Co2-O>		2.1385	1.068	1.071	0.372	1.701
<Co-O>		2.1282	1.063	1.066	0.383	1.714
Ni1	-O1	2.0685	1.039	1.029	0.442	1.832
	-O2	2.0677	1.038	1.031	0.452	1.840
	-O3	2.1038	1.055	1.050	0.419	1.801
<Ni1-O>		2.0800	1.044	1.037	0.438	1.824
Ni2	-O1	2.1085	1.058	1.051	0.403	1.785
	-O2	2.0350	1.024	1.011	0.465	1.861
	-O3	2.0570	1.035	1.022	0.442	1.835
	-O3'	2.1717	1.086	1.087	0.363	1.729
<Ni2-O>		2.1002	1.054	1.047	0.413	1.795
<Ni-O>		2.0901	1.049	1.042	0.425	1.810

Hence, in summary, the M1-O bonds appear on average less ionic in character than the M2-O bonds.

(3) Transition metal cations prefer the site that provides the larger crystal field stabilization energy (CFSE). The CFSE at M1 exceeds increasingly that at M2, from Mn^{2+} (CFSE = 0) to Fe^{2+}, to Co^{2+} and Ni^{2+} (Walsh *et al.*, 1976; Burns & Sung, 1978). In this context, Walsh *et al.* (1974) argue that the dynamic Jahn-Teller effect that favours partitioning of Fe^{2+} into M2 approximately outweighs the Fe^{2+} preference for M1 due to the CFSE.

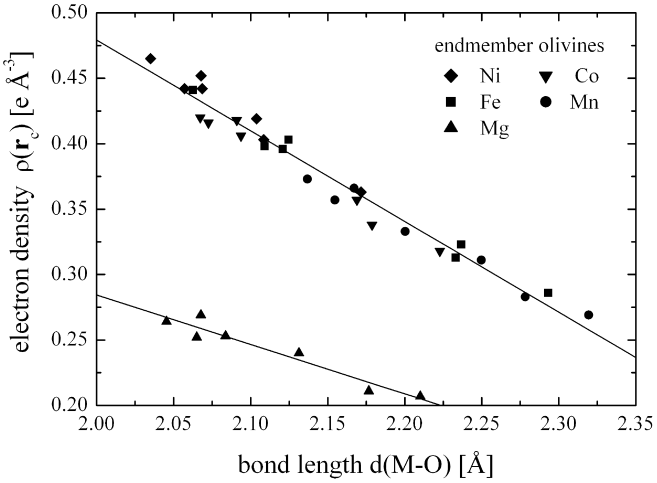

Fig. 6. Electron densities at the bond critical points, $\rho(\mathbf{r}_c)$ [e Å^{-3}], as a function of the respective bond lengths, d(M – O) [Å], of $M_2[SiO_4]$ olivine endmembers (M = Mn, Fe, Co, Ni, Mg).

Tsukimura & Sasaki (2000) suggested modelling $\ln K_D$ in terms of the above crystal-chemical factors. However, all these factors directly relate to the temperature-independent exchange enthalpy rather than to $\ln K_D$, which is temperature-dependent. Thus, for an appropriate description of $\ln K_D$, ΔS^0_{exch} has to be modelled as well.

Cation radii and electronegativities from procrystal electron density distributions

In order to investigate the relations between the exchange enthalpies on one hand and the bond specific radii and electronegativities of the two-valent cations on the other hand we have calculated total electron density distributions $\rho(\mathbf{r})$ for olivine endmember procrystals on the basis of neutral atom canonical wave functions (Clementi, 1965; Stewart & Spackman, 1983). In these calculations, atomic thermal displacements were neglected. The positional parameters were taken from own work or literature. Using the program package VALRAY 96 (Stewart *et al.*, 2000), which includes the option for topological analysis of the total model electron density distribution, results were obtained for olivines $M_2[SiO_4]$, with M = Mn, Fe, Co, Ni, Mg. For Mg, Fe and Co olivine, the structure data stem from own measurements with high-energy synchrotron radiation (Kirfel & Lippmann, 2001, 2002; Kirfel *et al.*, 2003; Gibbs *et al.*, 2005; Kirfel *et al.*, 2005), those for Mn and Ni olivine were taken from Fujino *et al.* (1981), and Boström (1989), respectively.

The topological analyses of the total model electron density distributions $\rho(\mathbf{r})$ comprised the calculation of bond critical points (bcp), where the gradient $\nabla\rho(\mathbf{r})$ vanishes (Ba-

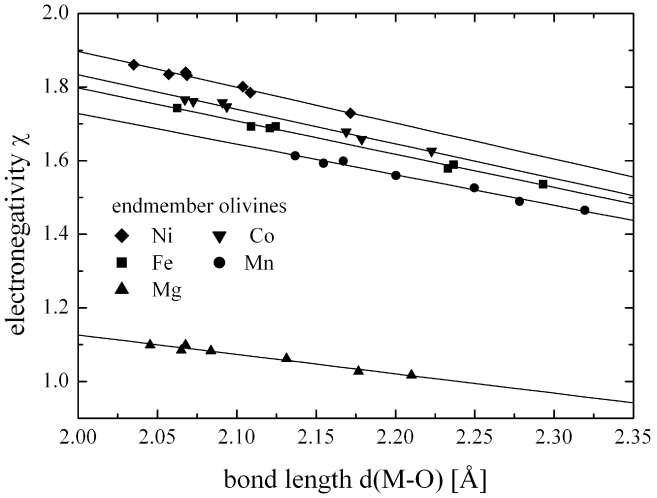

Fig. 7. Electronegativities, χ, obtained from equation (15) for individual bonds as a function of the respective bond lengths, d(M – O) [Å], of $M_2[SiO_4]$ olivine endmembers (M = Mn, Fe, Co, Ni, Mg).

der, 1990, 1998), and of the associated density distribution properties. Here, it suffices to consider the distances M-bcp and bcp-O which can be taken as the bonded radii r(M) and r(O) of the central cations and oxygen anions, respectively.

(3,-1) bond critical points were found on all M-O bonds. The distances from the associated bonded atoms to the bcp's and the density values at the bcp's are compiled in Table 2. Clearly, as the M-O bond length increases the density at the critical point, $\rho(\mathbf{r}_c)$, decreases in agreement with expectation (Fig. 6). Because all bonds contain covalent contributions, the cation radii in Table 2 are larger in magnitude than the well known ionic radii tabulated elsewhere, but the differences between the "new" bonded radii are completely unbiased by any crystal-chemical consideration, i.e. they are truly independent of all values traded in the literature.

The last column in Table 2 contains cation electronegativity values as estimated by the expression (Boyd & Edgecombe, 1988; Hill *et al.*, 1997),

$$\chi = 1.31\frac{N \cdot \rho(\mathbf{r}_c)^{0.23}}{r(O)} \qquad (15)$$

which makes the electronegativity a bond specific property. N is the number of valence electrons of the cation, e.g. 8 for Fe if the 3d-electrons are included. The procrystal values of χ for Mg are somewhat smaller than Pauling's value of 1.20, whereas the χ values for all the other cations are found to agree within some percent with the electronegativities given by Allred & Rochow (1958). In general, Table 2 and Fig. 7 indicate (i) increasing electronegativity differences between Mg and the transition metals as the number of 3d-electrons increases, and (ii) decreasing χ values as the bond distances increase. Hence, the M-O interactions become the more closed-shell in character the longer the bonds and the larger the electronegativity differences between Mg and its cation counterparts are.

A comparison of the data in Table 2 with corresponding results obtained after multipole refinements on the high-energy synchrotron radiation data quoted above shows that upon modelling the bond-induced charge redistribution both the density at the critical point and the oxygen bonded radius increase. As a consequence, the χ estimates obtained for the cations in the procrystal are only little changed by chemical bonding, i.e. due to the inherent correlation between $\rho(\mathbf{r}_c)$ and the anion bonded radius, r(O), the procrystal itself provides already reasonable estimates of bond specific electronegativities.

Table 3. Atomic basin volumes V [Å^3], equivalent sphere radii r_{eq} [Å], no. of electrons Z contained in V and formal atomic charges Q for the M1 and M2 sites in pure endmember olivines. Values are based on the zero flux criterion for space partitioning.

site	V [Å^3]	r_{eq} [Å]	Z	Q
Mg(M1)	5.943	1.124	10.60	1.403
Mn(M1)	12.100	1.424	23.96	1.040
Fe(M1)	11.277	1.391	25.00	1.000
Co(M1)	10.250	1.348	26.01	0.986
Ni(M1)	9.867	1.331	27.07	0.928
Mg(M2)	6.227	1.141	10.59	1.413
Mn(M2)	12.272	1.431	23.91	1.090
Fe(M2)	11.406	1.396	24.95	1.050
Co(M2)	10.530	1.360	25.98	1.020
Ni(M2)	10.137	1.343	27.04	0.965

Space partitioning into "atomic basins" can be achieved by analyzing the gradient vector field of the total model charge density distribution. These basins are defined by surfaces which are not crossed by gradient vectors, i.e. the "zero flux" criterion $\nabla\rho(\mathbf{r}) \cdot \mathbf{n}(\mathbf{r}) = 0$ holds for each surface point, $\mathbf{n}(\mathbf{r})$ being the surface normal vector (Bader, 1990). Using the space-partitioning algorithm implemented in VALRAY (Flensburg & Madsen, 2000) the calculations for the determination of the boundaries of the gradient field were carried out on the basis of 6 x 6 x 6 unit-cells and 96 Θ-planes and 72 radial integration steps yielding 6388 points on the surface. Once the resulting M1 and M2 basins are defined, the integrals of $\rho(\mathbf{r})$ yield the numbers of electrons contained in the basins and thus estimates of the atomic charges. Such charges result already from the mere superposition of the localized spherical atomic density distributions and are indicative of the bond characters. The results found for the olivines are compiled in Table 3. For all compounds, V(M1) < V(M2) is corroborated and concomitantly the cations at M2 are slightly more charged than those at M1. Thus, the earlier mentioned conclusions as to the nature of the bonding in M1 and M2 are fully confirmed by the analyses of the various density distributions that are exclusively based on structural parameters.

Modelling exchange enthalpies

In Table 4, average cation radii and electronegativities are calculated from the data of Table 2. Crystal field stabilization energies taken from the literature have been added. Before combining the crystal-chemical factors, we first examine their individual influences on the ordering behaviour. (a) When ΔCFSE is assumed the only factor determining site preferences, Table 4 indicates that MnMg olivine should

Table 4. Left: Mean cation radii r(M) [Å] and electronegativities χ for pure endmember olivines. Right: Radius ratios q[r(M)] and electronegativity ratios q(χ) as derived in this study, together with crystal field stabilisation energies taken from the literature.

M olivine	r(M) [Å]	χ	AB olivine	q[r(M)]	q(χ)	ΔCFSE [J/mol]	
Mn	1.115	1.550	MnMg	1.1943	1.4508	0	
Fe	1.091	1.650	FeMg	1.1680	1.5441	860	Burns & Sung, 1978
Co	1.063	1.716	CoMg	1.1381	1.6055	4160	Walsh *et al.*, 1976
Ni	1.049	1.810	NiMg	1.1232	1.6944	8130	Walsh *et al.*, 1976
Mg	0.934	1.069	MnFe	1.0226	0.9395		

r(M) and χ were calculated from Table 2 [when necessary the radii were normalized to give r(M) + r(O) = d(M-O)]; q[r(M)] = r(A) / r(B), q(χ) = χ(A) / χ(B); CFSE = crystal field stabilisation energy; $\Delta CFSE = CFSE(M^{2+}_{M1}) - CFSE(M^{2+}_{M2})$

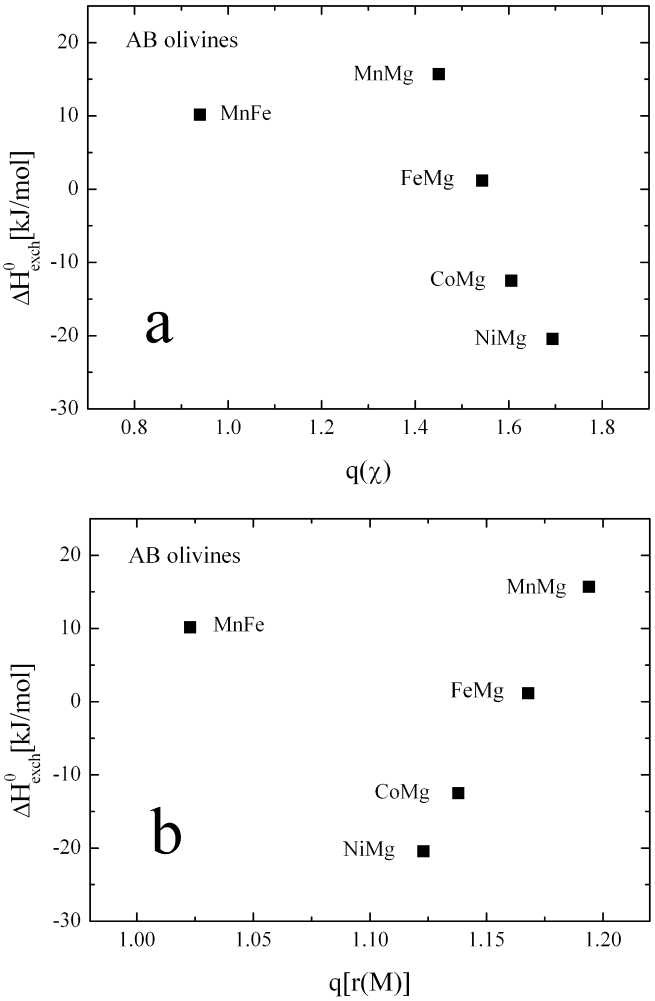

Fig. 8. Relation between exchange enthalpies, ΔH^0_{exch}, and (a) electronegativity ratios, q(χ), and (b) radius ratios, q[r(M)], of AB olivines.

be disordered, while FeMg, CoMg and NiMg olivines should be anti-ordered to increasing degrees. (b) The ratios of the electronegativities, q(χ) = χ(A)/χ(B), being larger than 1 for the MnMg to NiMg olivines (Fig. 8a) indicate that these compounds should be increasingly anti-ordered, while only MnFe olivine with q(χ) < 1 should be ordered. (c) Obviously, these tendencies do not agree with the observed order behaviour reflected by the magnitudes and signs of ΔH^0_{exch} in Table 1. Rather, another factor must outweigh the influences of ΔCFSE and q(χ), the obvious candidate being the radius ratio, q[r(M)] = r(A) / r(B), which decreases from MnMg to NiMg and MnFe olivine (Fig. 8b) so that these compounds should all be ordered, though to decreasing degrees. In fact, combining q[r(M)] and q(χ) the observed tendencies of order and anti-order are reproduced very satisfactorily. A weighted least-squares analysis of

$$\Delta H^0_{exch} = c_1\,[r(A)/r(B) - 1] + c_2\,[\chi(A)/\chi(B) - 1]$$

yields

$$\Delta H^0_{exch} = 252.6(\pm 6.1)\,[r(A)/r(B) - 1] - 75.8(\pm 1.9)\,[\chi(A)/\chi(B) - 1]. \quad (16)$$

The constant 1 has to be subtracted from q[r(M)] and q(χ) in order to correctly predict $\Delta H^0_{exch} = 0$ for the pure endmember olivines with both ratios equalling 1. Since ΔCFSE is related to q[r(M)] and q(χ), it is implicitly incorporated in equation (16). Figure 9 shows that in FeMg olivine the almost equal but opposing crystal-chemical factors of electronegativity and cation radius nearly cancel so that only a very small positive site preference enthalpy of 1.2 kJ/mol remains which manifests itself in a very small ordering tendency. In comparison, MnMg and MnFe olivines on one hand, and CoMg and NiMg olivines on the other hand are correctly predicted to adopt exclusively ordered and anti-ordered states, respectively.

With respect to the modelling of $\ln K_D$ in terms of equation (12), one may consider the possibility that the exchange enthalpy itself might depend on temperature. This being true, a linear dependence of ΔH^0_{exch} on T would be camouflaged by the ΔS^0_{exch} term. However, the rationalization of ΔH^0_{exch} in terms of cation radii and electronegativity ratios makes it rather unlikely that this energy should significantly depend on temperature and as such drive an ordered state towards anti-order or vice versa (also see Wu & Mason, 1981).

Finally, a question briefly evoked is whether the results of the procrystal electron density calculations are really suited to serve as substitutes for the results of more detailed density analyses that are based on multipole refinements aiming at modelling chemical bond induced charge redistribution. For a comparison, results of two such analyses carried out with high-energy synchrotron radiation data were considered, one on forsterite, the other one on fayalite (Kirfel & Lippmann, 2001, 2002; Kirfel *et al.*, 2003; Gibbs *et al.*, 2005;

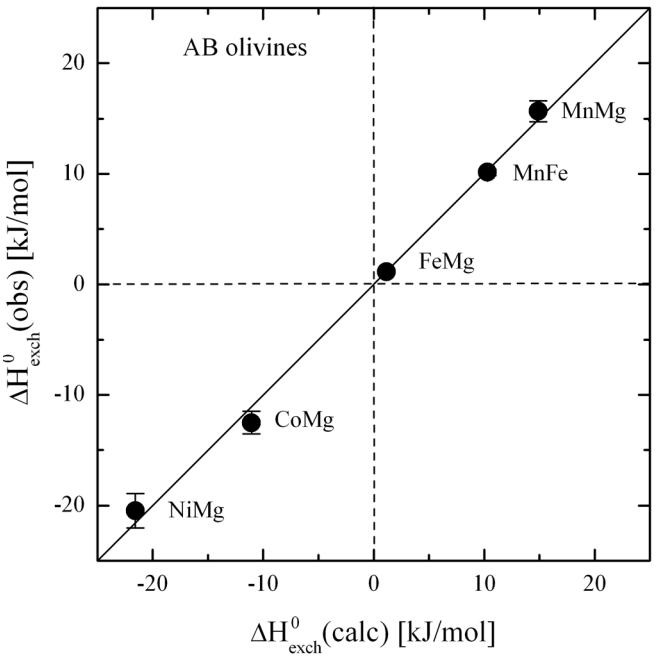

Fig. 9. Exchange enthalpies, ΔH^0_{exch}, of AB olivines calculated from a linear combination of ionic radii and electronegativity ratios (eqn 16) compared with their observed counterparts.

Kirfel *et al*., 2005). The original two parameters used for modelling ΔH^0_{exch} changed only little for FeMg olivine: q[r(M)] from 1.168 to 1.162 and likewise q(χ) from 1.544 to 1.543 (compare Table 4). Accordingly, working with the results of procrystal density calculations appears reasonable and justified (see also Gibbs *et al*., 1997; Tirelson *et al*., 1998; Downs *et al*., 2002).

Modelling exchange entropies

The nonconfigurational entropy difference, ΔS^0_{exch}, between the anti-ordered and ordered states is thought to be a consequence of the vibrational frequency change, $\Delta S^{0,vib}_{exch}$, associated with the cation interchange (Kröger, 1964; Wu & Mason, 1981). Wu & Mason content that such a frequency change may arise from the expansion of one sublattice and the simultaneous contraction of the other. According to this view, a suitable model for $\Delta S^{0,vib}_{exch}$ could possibly be based on the ratio of the sum of the cation radii in the anti-ordered $B^{M2}A^{M1}$ and ordered $A^{M2}B^{M1}$ configurations,

$$\Delta S^{0,vib}_{exch} \sim \{[r(B)^{M2} + r(A)^{M1}] / [r(A)^{M2} + r(B)^{M1}] - 1\} \qquad (17)$$

where $r(A)^{M1}$, etc. are the radii of the A and B cations in the M1 and M2 sites, respectively, as given in Table 4. We found, however, this approach to be unsatisfactory.

Another factor that is likely to be related to $\Delta S^{0,vib}_{exch}$ is octahedral site distortion. When a cation moves from a distinctly distorted octahedral site to another, differently distorted one, the vibrational behaviour of the cation should be affected. In olivines, the deviations of the octahedral bond lengths from ideal are larger for the site M2 than for M1, while the reverse applies to the bond angles. For our purpose, it is desirable to employ a parameter that reflects both the length and angle variances and thus improves the description of the different distortion characteristics of the two sites. Such a parameter was proposed by Sutanto (2004) and Sutanto *et al.* (2004) who introduced the normalized standard deviation, D_f, of the eight triangular faces of the cation coordination octahedron,

$$D_f = \frac{\sqrt{\Sigma(p_i - \bar{p})^2/8}}{\bar{p}} \qquad (18)$$

where p is the triangular face area. Values of the face distortion parameters, $D_f(A,B)^{M1,2}$, of the A and B cations in the M1 and M2 sites, respectively, were calculated from the same endmember olivines that were used in the procrystal density calculations (Table 5). In analogy to equation (17), these values can then be used for describing $\Delta S^{0,vib}_{exch}$ in terms of the face distortion ratio,

$$\Delta S^{0,vib}_{exch} \sim \{[D_f(B)^{M2} + D_f(A)^{M1}] / [D_f(A)^{M2} + D_f(B)^{M1}] - 1\}. \qquad (19)$$

An additional factor contributing to ΔS^0_{exch} comes into play when A or B is a transition metal atom, i.e. the electronic exchange entropy, $\Delta S^{0,el}_{exch}$,

$$\Delta S^0_{exch} = \Delta S^{0,vib}_{exch} + \Delta S^{0,el}_{exch}. \qquad (20)$$

According to Burns & Sung (1978) the five-fold degeneracy of the 3d-orbitals of a free transition metal ion vanishes when the ion centres a distorted M1 or M2 octahedron in olivine. The five 3d-orbitals are then split into three low level t_{2g} and two high level e_g orbitals. In the Fe^{2+} ion, for example, five of the six 3d-electrons occupy the five t_{2g} and e_g levels, one each. At 0 K, the sixth electron is located at the lowest level t_{2g} orbital. At increasing temperatures it obtains an increasingly random distribution over the three t_{2g} levels following the Boltzmann distribution. The entropy contribution of this electron can be calculated according to the scheme,

$$S^{el} = -R\sum_{i=1}^{3} p_i \ln p_i \qquad (21)$$

where $p_i = A_i / Z$, $A_i = \exp(-E_i / k_B T)$, $Z = \sum_{i=1}^{3} A_i$.

R is the gas constant, k_B the Boltzmann constant and E_i are energy differences between the t_{2g} levels of the M1 and

Table 5. Left: Octahedral face distortion parameters D_f of pure endmember olivines. Right: Face distortion ratios $q(D_f)$ and electronic exchange entropies $\Delta S^{0,el}_{exch}$ of intermediate compounds.

M olivine	D_f(M1)	D_f(M2)	AB olivine	$q(D_f)$	$\Delta S^{0,el}_{exch}$ [J/mol K]
Mn	0.1136	0.0760	MnMg	1.0753	0
Fe	0.1069	0.0670	FeMg	1.0944	0.3
Co	0.0970	0.0658	CoMg	1.0397	0.2
Ni	0.0891	0.0638	NiMg	1.0029	0
Mg	0.0925	0.0676	MnFe	0.9870	-0.3

$q(D_f) = [D_f(A)^{M1} + D_f(B)^{M2}] / [D_f(B)^{M1} + D_f(A)^{M2}]$

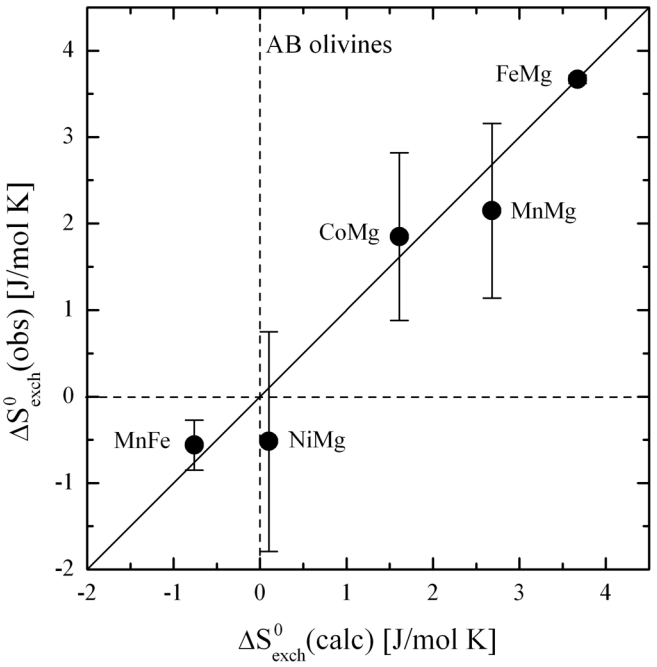

Fig. 10. Exchange entropies, ΔS^0_{exch}, of AB olivines calculated from a linear combination of the ratio of face distortion parameters and the electronic exchange entropy (eqn 22) compared with their observed counterparts.

M2 sites, respectively. Values for fayalite have been reported by Burns & Sung (1978) and we assume that they can be transferred to Fe^{2+} in FeMg and MnFe olivine. Since the energy differences are smaller for the M1 than for the M2 site, $\Delta S^{0,el}_{exch} = S^{0,el}_{Q=-1} - S^{0,el}_{Q=-1}$ is positive for FeMg olivine, whereas it is negative for MnFe olivine (Table 1). Calculation of $\Delta S^{0,el}_{exch}$ reveals that it depends on temperature; an (absolute) average value of 0.30 J/molK is a good approximation. The t_{2g} energy levels of the Co^{2+} ion are not known and were approximated by the fayalite data. Co^{2+} has seven 3d-electrons, two of which can be distributed over the three t_{2g} levels. The calculation yields $\Delta S^{0,el}_{exch} \approx 0.20$ J/molK for CoMg olivine. For Mn^{2+} and Ni^{2+} with five and eight 3d-electrons, respectively, $\Delta S^{0,el}_{exch} = 0$ J/molK. Including $\Delta S^{0,el}_{exch}$ into equation (19) the weighted regression of ΔS^0_{exch} slightly improved the fit yielding

$$\Delta S^0_{exch} = 35.76(\pm 0.34)\ \{[D_f(B)^{M2} + D_f(A)^{M1}] / [D_f(A)^{M2} + D_f(B)^{M1}] - 1\} + \Delta S^{0,el}_{exch} \quad (22)$$

The agreement obtained between the observed and calculated ΔS^0_{exch} values is illustrated in Fig. 10.

Comparison of modelled and observed site occupancies

Model site occupancies were obtained from equation (12) after insertion of equations (16) and (22). The results represented by the model curves in Fig. 11 show that the site occupancies calculated from the crystal-chemical model reproduce the observed values within 1σ to 3σ, depending on the particular olivine.

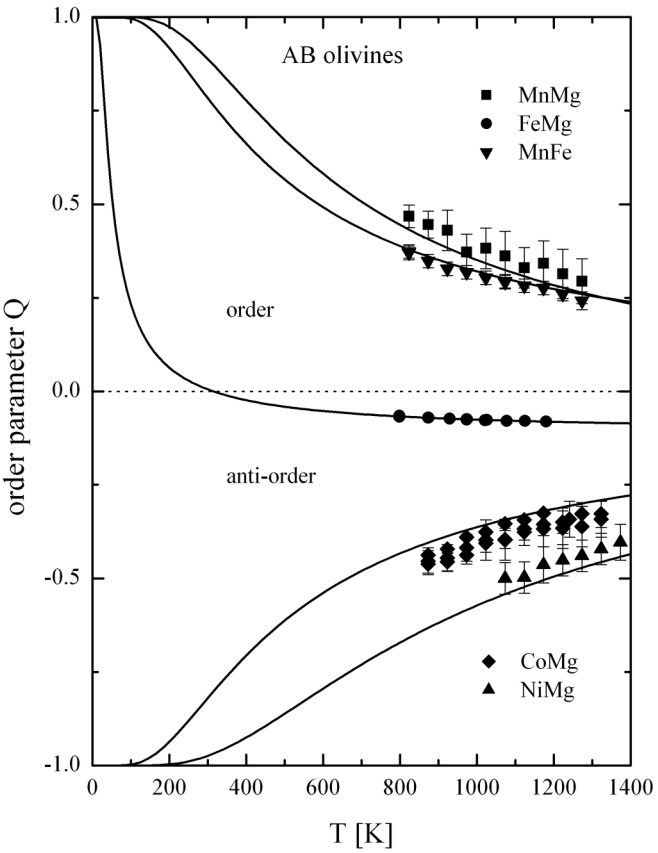

Fig. 11. Variation with temperature of the order parameter $Q = X^{M2}_A - X^{M1}_A$ (A = Mn, Fe, Co, Ni). X^{M1}_A and X^{M2}_A are site occupancies calculated from equation (12) using the modelled ΔH^0_{exch} (eqn 16) and ΔS^0_{exch} (eqn 22) relations. The predicted variations of Q mostly agree with the observations within 1σ to 3σ. The data points for CoMg olivine represent three different measurements (Sutanto, 2004).

Table 6. Five olivine endmembers and ten intermediate AB olivines resulting from the combination of the five cations Mn, Fe, Co, Ni, Mg. Bold face: yet unexplored AB olivines.

	Mn	Fe	Co	Ni	Mg
Mn	MnMn	MnFe	**MnCo**	**MnNi**	MnMg
Fe		FeFe	**FeCo**	**FeNi**	FeMg
Co			CoCo	**CoNi**	CoMg
Ni				NiNi	NiMg
Mg					MgMg

Prediction of temperature dependent site occupancies in yet unexplored AB olivines

Table 6 lists the ten AB olivines that could possibly be synthesized from a combination of the five elements Mg, Mn, Fe, Co, Ni. The ordering behaviour of five of them has been discussed above. The behaviour of the other five compounds is unknown, but may be predicted from the model. Inserting the appropriate radius and electronegativity ratios into equation (16) yields the values of ΔH^0_{exch} given in Table 7 and shown in Fig. 12a,b. All five exchange enthalpies are positive with ΔH^0_{exch} of MnNi olivine being largest, that of CoNi olivine being smallest. Since in those compounds the

Table 7. Left: Mean cation radii r(M) [Å] and electronegativities χ for pure endmember olivines. Right: Radius ratios q[r(M)] and electronegativity ratios q(χ) used to predict from equation (16) exchange enthalpies ΔH^0_{exch} of five olivines not yet thermally investigated. Face deformation ratios $q(D_f)$ and exchange electronic entropies $\Delta S^{0,el}_{exch}$ used to predict exchange entropies ΔS^0_{exch} from equation (22).

M olivine	r(M) [Å]	χ	AB olivine	q[r(M)]	q(χ)	ΔH^0_{exch} (pred.) [kJ/mol]	$q(D_f)$	$\Delta S^{0,el}_{exch}$ [J/mol K]	ΔS^0_{exch} (pred.) [J/mol K]
Mn	1.115	1.550	MnNi	1.063	0.856	26.9	1.074	0	2.6
Fe	1.091	1.650	FeNi	1.040	0.911	16.8	1.094	0.3	3.6
Co	1.063	1.716	CoNi	1.013	0.948	7.3	1.038	0.2	1.5
Ni	1.049	1.810	MnCo	1.049	0.904	19.8	1.037	–0.2	1.1
Mg	0.934	1.069	FeCo	1.026	0.962	9.5	1.054	0.1	2.0

r(M) and χ were calculated from Table 2 [when necessary the radii were normalized to give r(M) + r(O) = d(M-O)]; q[(r(M)] = r(A) / r(B), q(χ) = χ(A) / χ(B), $q(D_f = [D_f(A)^{M1} + D_f(B)^{M2}] / [D_f(B)^{M1} + D_f(A)^{M2}]$

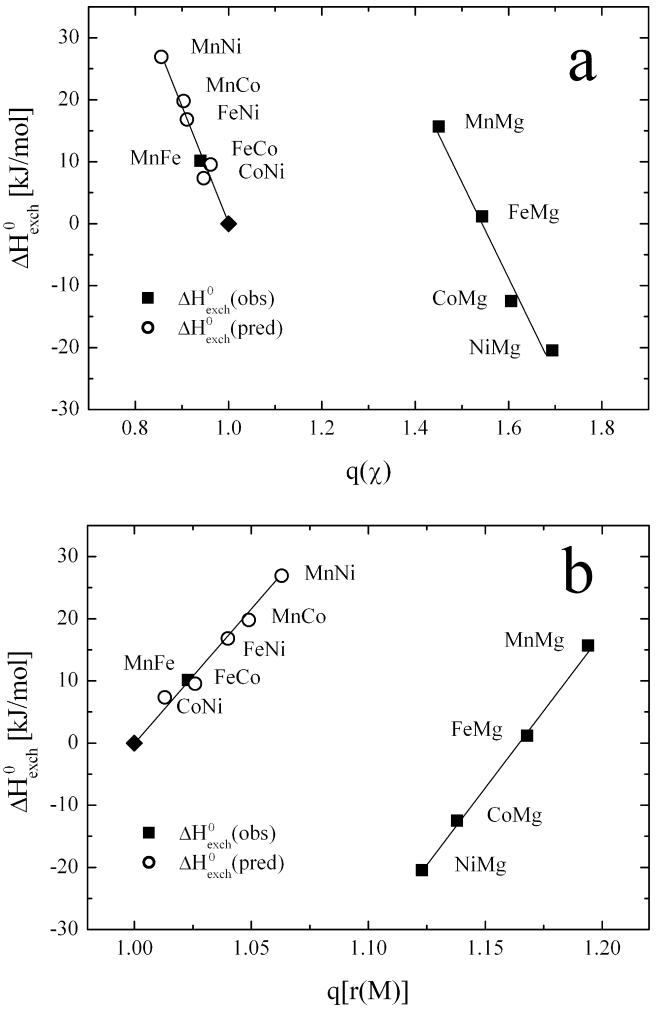

Fig. 12. Relation between exchange enthalpies, ΔH^0_{exch}, predicted by our crystal-chemical model (eqn 16) for AB olivines that have not yet been thermally investigated and (a) their electronegativity ratios, q(χ), and (b) their radius ratios, q[r(M)] (open dots). Observed data have been added for comparison (filled squares). The filled diamond symbolizes ΔH^0_{exch} of endmember olivines.

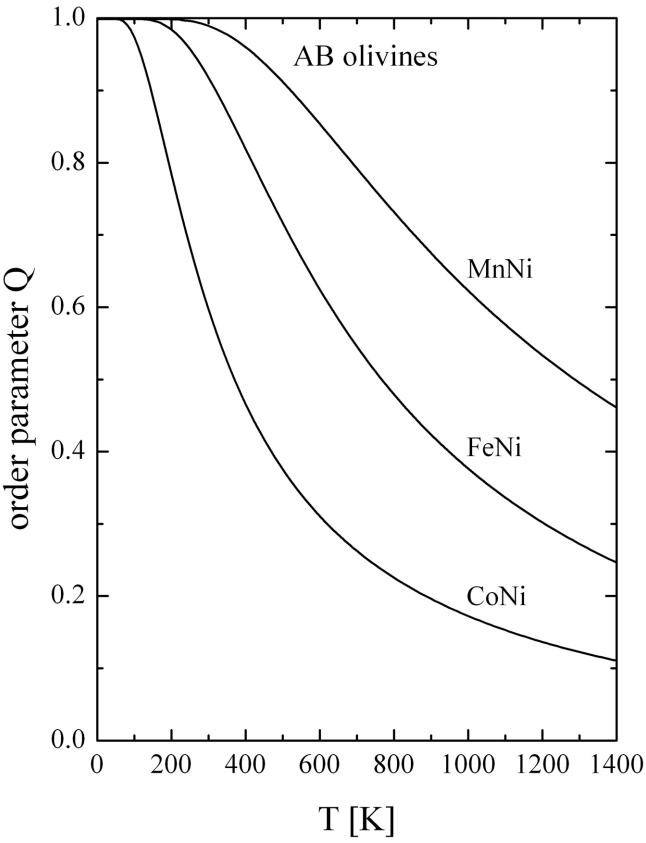

Fig. 13. Variation with temperature of the order parameter $Q = X_A^{M2} - X_A^{M1}$ (A = Mn, Fe, Co) predicted from our crystal-chemical model (eqns 16 and 22) for MnNi, FeNi and CoNi olivines, not investigated thermally, so far.

radius ratio q[r(M)] is larger than 1 while the electronegativity ratio q(χ) is smaller than 1, both effects are additive. As a consequence, the A cation prefers M2 due to its larger radius and smaller electronegativity, while at the same time, the B cation prefers M1 due to its smaller radius and larger electronegativity. Both q[r(M)] and q(χ) approach 1 applying to the endmember compounds. Figure 13 shows examples of the temperature variation of the order parameter Q predicted from equation (12). It illustrates (a) the effect of the decreasing exchange enthalpy on Q(T) as q[r(M)] and q(χ) approach 1 and (b) the influence of the exchange entropy on the curvature of Q(T).

The transition metal – Mg olivines behave differently because both q[r(M)] and q(χ) exceed 1. This implies that the transition metal atoms prefer M2 due to their larger radii and

simultaneously prefer M1 due to their larger electronegativity values (the opposite holds for Mg). Thus, in contrast to the pure transition metal olivines both effects are antagonistic. For MnMg olivine, the radius effect dominates and thus stabilizes order, for FeMg olivine both effects nearly cancel so that these olivines are close to disorder at all temperatures, and for CoMg and NiMg olivine the larger electronegativity effect stabilizes anti-order (Fig. 4).

Discussion and Conclusion

The idea of an increasing order or anti-order at increasing temperature seems to be strange at first sight. In general, increasing temperature results in increasing rather than decreasing configurational entropy. However, a decrease of the configurational entropy appears possible when its positive contribution to the Gibbs energy is counterbalanced by another contribution that is larger and negative. Artioli *et al.* (1995), Rinaldi *et al.* (2000) and Redfern *et al.* (2000) have reported a reverse ordering reaction taking place in Fe,Mg olivine at elevated temperatures and leading to significant repartitioning of Fe^{2+} into M2 after an initial preference for M1. They explain this behaviour by a large increase of the vibrational entropy which overrides the effect of decreasing configurational entropy. This raises, however, the question why the vibrational entropy should suddenly increase. In olivine Fa48, Heinemann *et al*. (2003a,b; 2006) could not confirm such a reverse ordering. In our study, we relate the continuing fractionation of Fe^{2+} into M1 to the difference of the nonconfigurational entropies between anti-ordered and ordered Fe^{2+},Mg configurations due to which at increasing temperature anti-ordered states (Fe^{2+} segregating into M1) are preferred over ordered states (Fe^{2+} partitioning into M2). Such behaviour is allowed thermodynamically and in principle is not restricted to olivine. It is, however, not observed in other minerals (except for magnetite) because the site exchange enthalpy is generally too large to allow the antagonistic nonconfigurational exchange entropy to come into play.

We have shown that crystal-chemical properties derived from pure endmember olivines are well suited to model experimentally obtained exchange enthalpies and entropies of intermediate AB olivines. The correlation coefficients of the regression analyses of ΔH^0_{exch} and ΔS^0_{exch} are $R^2 = 0.996$ and 0.933, respectively. For ΔH^0_{exch}, the excellent agreement between the modelled and observed values was only achieved by applying properties derived from the electron density distributions, i.e. cation-bcp radii and bond-specific electronegativities. The use of conventional radii and electronegativities yielded less satisfactory results. The agreement also declined when cation radii and electronegativities were substituted by other density properties like the oxygen-bcp radii, the density values at the bond critical points or the curvatures of the density at those points.

The exchange vibrational entropy could be successfully modelled using the octahedral face variance, which at first sight appears to be a purely geometrical factor. However, the distortions of the octahedra are in fact also intimately related to the electron density distribution since the atomic positions are defined by the (3,-3) critical points (density maxima). Thus, in the end, we can conclude that predictions of the temperature variation of the site occupancies in AB olivines can be derived from the procrystal electron density distributions of their pure endmember compounds.

Acknowledgements: This work was supported by grants of the Deutsche Forschungsgemeinschaft given to Herbert Kroll and Armin Kirfel, which is gratefully acknowledged. A. K. also gratefully acknowledges partial support of the electron density studies by the Minister of Education and Research (BMBF), contract Nr. 05KS1PDA. Our thanks are also due to Marc Hirschmann and an anonymous referee whose constructive reviews contributed to improve the manuscript.

References

Aikawa, N., Kumazawa, M., Tokonami, M. (1985): Temperature dependence of intersite distribution of Mg and Fe in olivine and the associated change of lattice parameters. *Phys. Chem. Minerals*, **12**, 1–8.

Allred, A.L. & Rochow, E. (1958): A scale of electronegativity based on electrostatic force. *J. Inorg. Nucl. Chem.*, **5**, 264–268

Artioli, G., Rinaldi, R., Wilson, C., Zanazzi, P.F. (1995): High-temperature Fe-Mg cation partitioning in olivine: In-situ single-crystal neutron diffraction study. *Am. Mineral.*, **80**, 197–200.

Bader, R.F.W. (1990): Atoms in molecules. Oxford Science Publications. Oxford.

– (1998): A bond path: universal indicator of bonded interactions. *J. Phys. Chem.*, **92A**, 7314–7323.

Bish, D.L. (1981): Cation ordering in synthetic and natural Ni-Mg olivine. *Am. Mineral.*, **66**, 770–776.

Boström, D. (1989): Cation ordering at 1300 °C in the (Ni,Mg)-olivine solid solution series. *Acta Chem. Scand.*, **43**, 116–120.

Boyd, R.J. & Edcombe, K.E. (1988): Atomic and group electronegativities from the electron density distributions of molecules. *J. Am. Chem. Soc.*, **19**, 4182–4186.

Brown, G.E. Jr (1980): Olivines and silicate spinels. In: Orthosilicates. Reviews in Mineralogy, Vol. 5, 275–381, Mineralogical Society of America.

Burns, R.G. (1970): Crystal field spectra and evidence of cation ordering in olivine minerals. *Am. Mineral.*, **55**, 1608–1632.

Burns, R.G. (1983): Mineralogical applications of crystal field theory. 2nd ed., Cambridge University Press, XIII, 551 p.

Burns, R.G. & Sung, Ch.-M. (1978): The effect of crystal field stabilization on the olivine → spinel transition in the system Mg_2SiO_4-Fe_2SiO_4. *Phys. Chem. Minerals*, **2**, 349–364.

Clementi, E. (1965): Tables of atomic functions. *IBM J. Res. Dev.*, **9**, (Suppl.).

Downs, R.T., Gibbs, G.V., Boison, M.B. Jr., Rosso, K.M. (2002) Comparison of procrystal and ab initio model representations of the electron density of minerals. *Phys. Chem. Minerals*, **29**, 369–385.

Finger, L.W. & Virgo, D. (1971): Confirmation of Fe/Mg ordering in olivines. *Carnegie Inst. Washington Yearbook*, **70**, 221–225.

Flensburg, C. & Madsen, D. (2000): Atoms in crystals – from experimental charge densities. *Acta Cryst.* **A56**, 24–28.

Freiheit V., Heinemann R., Kroll H., Krane H.-G., Kirfel A. (2000): Thermal history of natural olivines from the temperature dependent cation distribution determined by laboratory and synchro-

tron radiation X-ray diffraction. *HASYLAB*, Annual Report, 2000.

Fujino, K., Sasaki, S., Takeuchi, Y., Sadanaga, R. (1981): X-ray determination of electron density distributions in forsterite, fayalite and tephroite. *Acta Cryst.*, **B37**, 513–518.

Gibbs, G.V., Tamada, O., Boison, M.B. Jr. (1997) Atomic and ionic radii: comparison with radii derived from electron density distributions. *Phys. Chem. Minerals*, **24**, 432–439.

Gibbs, G.V., Cox, D.F., Rosso, K.M., Kirfel, A., Lippmann, T., Blaha, P., Schwarz, K. (2005): Experimental and theoretical bond critical point properties for model electron density distributions for earth materials. *Phys. Chem. Minerals*, **32**, 114–125.

Ghose, S. (1982): Mg-Fe order-disorder in ferromagnesian silicates. I. Crystal Chemistry. In: S.K. Saxena, Ed., Advances in Physical Geochemistry, **2**, 4–57, Springer, New York.

Heinemann, R., Kroll, H., Kirfel, A., Barbier, B. (2003a): Die kontroverse Diskussion des Ordnungsverhaltens von Fe^{2+} und Mg in Olivinen. *Mitt. Österr. Mineral. Ges.*, **148**, 159–160.

–,– (2003b): Die Temperaturabhängigkeit der Fe^{2+},Mg-Verteilung in Olivinen. *Berichte der Deutschen Mineral. Gesellschaft, Beih. zum Eur. J. Mineral.*, **15**, 78, No 1.

–,– (2006) Order and anti-order in olivines I: Structural response to temperature. *Eur. J. Mineral.,* **18**, 673–689.

Henderson, C.M.B., Redfern, S.A.T., Smith, R.I., Knight, K.S., Charnock, J.M. (2001): Composition and temperature dependence of cation ordering in Ni-Mg olivine solid solutions: a time-of-flight neutron powder diffraction and EXAFS study. *Am. Mineral.*, **86**, 1170–1187.

Hill, F.C., Gibbs, G.V., Boisen, M.B. (1997): Critical point properties of electron density distributions for oxide molecules containing first and second row cations. *Phys. Chem. Minerals*, **24**, 582–596.

Kirfel, A. & Lippmann, T. (2001): Charge density study of forsterite, Mg_2SiO_4. *HASYLAB*, Annual Report, 449–450.

–,– (2002): Electron Density Distribution in Fayalite, Fe_2SiO_4: a high-energy synchrotron radiation study. *HASYLAB*, Annual Report, 515–516.

Kirfel, A., Lippmann, T., Morgenroth, W. (2003): Electron density distribution in tephroite, Mn_2SiO_4: A high-energy synchrotron radiation study. *HASYLAB*, Annual Report, 601–602.

Kirfel, A., Lippmann, T., Blaha, P., Schwarz, K., Cox, D.F., Rosso, K.M., Gibbs, G.V. (2005): Electron density distribution and bond critical properties for forsterite, Mg_2SiO_4, determined with synchrotron radiation single crystal X-ray diffraction data. *Phys. Chem. Minerals*, **32**, 301–313.

Kröger, F.A. (1964): The chemistry of imperfect crystals. North-Holland Publishing, Amsterdam.

Kroll, H., Schlenz, H., Phillips, M.W. (1994): Thermodynamic modelling of non-convergent ordering in orthopyroxenes: A comparison of classical and Landau approaches. *Phys. Chem. Minerals*, **21**, 555–560.

Kroll, H., Lueder, T., Schlenz, H., Kirfel, A., Vad, T. (1997): The Fe^{2+},Mg distribution in orthopyroxene: A critical assessment of its potential as a geospeedometer. *Eur. J. Mineral.*, **9**, 705–733.

Miyake, M., Nakamura, H., Kojima, H., Marumo, F. (1987): Cation ordering in Co-Mg olivine solid-solutions series. *Am. Mineral.*, **72**, 594–598

Morozov, M., Brinkmann, C., Kroll, H., Lottermoser, W., Tippelt, G., Amthauer, G. (2001a): Mössbauer effect study of the Mg^{2+},Fe^{2+}-distribution in synthetic olivine (fa50 fo50). *Berichte der Deutschen Mineral. Gesellschaft, Beih. zum Eur. J. Mineral.*, **13**, 127, No 1.

–,– (2001b): Mössbauerspektroskopische Untersuchung an Mg^{2+},Fe^{2+}-Verteilung in synthetischen Olivinen (fa50 fo50). *Mitt. Österr. Mineral. Ges.*, **146**, 202–203.

–,– (2002): Mg^{2+},Fe^{2+}-distribution in synthetic olivine ($Fa_{50}Fo_{50}$). Mineralogy for the New Millenium. 18th general meeting of the International Mineralogical Association. 1.–6. September 2002, Edinburgh, Scotland. *Programme with Abstracts*, 86.

Morozov, M., Brinkmann, C., Lottermoser, W., Tippelt, G., Amthauer, G., Kroll, H. (2005): Octahedral cation partitioning in Mg,Fe^{2+}-olivine. Mössbauer spectroscopic study of synthetic $(Mg_{0.5}Fe^{2+}{}_{0.5})_2SiO_4(Fa_{50})$. *Eur. J. Mineral.*, **17**, 495–500

Rajamani, V., Brown, G.E., Prewitt, C.T. (1975): Cation ordering in Ni-Mg olivine. *Am. Mineral.*, **60**, 292–299.

Redfern, S.A.T., Henderson, C.M.B., Knight, K.S., Wood, B.J (1997): High-temperature order-disorder in $(Fe_{0.5}Mn_{0.5})_2SiO_4$ and $(Mg_{0.5}Mn_{0.5})_2SiO_4$ olivines: An in situ neutron diffraction study. *Eur. J. Mineral.*, **9**, 287–300.

Redfern, S.A.T., Artioli, G., Rinaldi, R., Henderson, C.M.B., Knight, K.S., Wood, B.J. (2000): Octahedral cation ordering in olivine at high temperature. II: An in situ neutron powder diffraction study on synthetic $MgFeSiO_4$ (Fa50). *Phys. Chem. Minerals*, **27**, 630–637.

Rinaldi, R. Artioli, G., Wilson, C.C., McIntyre, G. (2000): Octahedral cation ordering in olivine at high temperature. I: In situ neutron single-crystal diffraction studies on natural mantle olivines (Fa12 and Fa9). *Phys. Chem. Minerals*, **27**, 623–629.

Sack, R.O. & Ghiorso, M.S. (1989): Importance of considerations of mixing properties in establishing an internally consistent thermodynamic database: Thermochemistry of minerals in the system Mg_2SiO_4-Fe_2SiO_4-SiO_2. *Contrib. Mineral. Petrol.*, **92**, 41–68.

Salje, E.K.H. (1992): Application of Landau theory for the analysis of phase transitions in minerals. *Physics Reports*, **215**, 49–99.

Shannon, R.D. & Prewitt, C.T. (1970): Effective ionic radii in oxides and fluorides. *Acta Cryst*., **B25**, 925–946.

Shannon, R.D. (1976): Revised effective ionic radii and systematic studies of interatomic distances in halides and chalcogenides. *Acta Cryst.*, **A32**, 751–767.

Shinno, I., Hayashi, M., Kuroda, Y. (1974): Mössbauer studies of natural olivines. *Min. Journ.*, **7**, 344–358.

Stewart, R.F., Spackman, M.A. (1983): VALRAY User's Manual, Carnegie-Mellon University, Pittsburgh PA.

Stewart, R.F., Spackman, M.A., Flensburg, C. (2000): VALRAY User's Manual, Version 2.1, Carnegie-Mellon University & University of Copenhagen, Pittsburgh PA.

Sutanto, R.P. (2004): Untersuchungen zur Temperaturabhängigkeit der Kationenverteilung in $CoMg[SiO_4]$. Diploma Thesis, Mineralogisches Institut der Universität Bonn, 87 pp

Sutanto, R.P., Kockelmann, W., Kirfel, A. (2004): Time resolved equilibration of the cation distribution in olivine type $(Co_{0.51}Mg_{0.49})_2SiO_4$. *Gemeinsame Jahrestagung DGK und DGKK. Referate*, Oldenbourg-Verlag, München.

Tamada, O. & Tanaka, K. (1988): Ionicity affecting the intracrystalline distributions in olivines in comparison with those in orthopyroxenes. *Mineral. Journ*., **14**, 12–19.

Tirelson, O., Abramov, Y., Zavodnik, V., Stash, A., Belekoneva, E., Stahn, J., Pietsch, U., Feil, D. (1998) Critical points in a crystal and procrystal. *Structural chemistry*, **9**, no.4, 249–254

Thompson, J.B. Jr (1969): Chemical reactions in crystals. *Am. Mineral.*, **54**, 341–375.

– (1970): Chemical reactions in crystals: Corrections and clarification. *Am. Mineral.*, **55**, 528–532.

Tsukimura, K. & Sasaki, S. (2000): Determination of cation distribution in $(Co,Ni,Zn)_2SiO_4$ olivine by synchrotron X-ray diffraction. *Phys. Chem. Minerals*, **27**, 234–241.

Walsh, D., Donnay, G., Donnay, J.D.H. (1974): Jahn-Teller effects in ferro-magnesian minerals. *Bull. Sc. Fr. Minéral. Crist.*, **97**, 170–183.

–,– (1976): Ordering of transition metal ions in olivine. *Can. Mineral.*, **14**, 149–150.

Wißmann, S., v. Wurmb, V., Litters, F.J., Dieckmann, R., Becker, K.D. (1998): The temperature dependent cation distribution in magnetite. *J. Phys. Chem. Solids*, **59**, 321–330

Wu, C.C. & Mason, T.O. (1981): Thermopower measurement of cation distribution in magnetite. *J. Amer. Cer. Soc.*, **64**, 520–522.

Received 26 March 2005
Modified version received 1 December 2005
Accepted 15 September 2006